Raman scattering of polaritons in crystals with large longitudinal-transverse exciton splitting

A. A. Maksimov and I. I. Tartakovski

Solid State Physics Institute, USSR Academy of Sciences
(Submitted 7 April 1988)
Zh. Eksp. Teor. Fiz. **94**, 293–304 (December 1988)

Using a tunable dye laser we studied secondary emission of anthracene crystals at low temperatures under resonance excitation conditions. We show that all the observed peculiarities of the secondary emission are connected with processes of propagation and scattering of polaritons by optical and acoustic phonons in a crystal with a large longitudinal-transverse exciton splitting. We obtain good quantitative agreement between experimental results and the polariton model.

1. INTRODUCTION

In the past few years, papers on the investigation of various polariton effects in the vicinity of the exciton resonance have occupied an important place in the investigation of optical properties of crystals possessing strong excitonic optical transitions. It is well known that in the presence of the exciton-photon interaction the intrinsic elementary excitations of these crystals become polaritons.[1,2] Polaritons possess a single dispersion curve which in the vicinity of the exciton resonance consist of two branches (curves I and II on Fig. 1; ω_T and ω_L correspond to the positions of the bottoms of the transverse and longitudinal mechanical exciton bands, respectively); in the approximation of a single nondegenerate exciton band, this curve can be described by an equation of the form

$$k^2 = \frac{\omega^2}{c^2}\varepsilon_0\left[1 - \frac{2\omega_T\omega_{LT}\sin^2\theta}{\omega^2 - \omega^2(\mathbf{k})}\right], \qquad (1)$$

where $\mathbf{k}$ is the polariton quasimomentum, ε_0 is the dielectric constant far from the resonance region, $\omega(\mathbf{k})$ is the energy of a mechanical exciton with wave vector $\mathbf{k}$, $\omega_{LT} = \omega_L - \omega_T$ is the magnitude of the longitudinal-transverse exciton splitting, θ is the angle between the vector $\mathbf{k}$ and $\mathbf{d}$, the dipole transition moment.

Within the framework of the polariton model, it is possible to describe diverse spectral and kinetic features in the secondary emission of crystals in a unified way. In the majority of cases, investigations have been carried out on direct-gap semiconductor crystals (see, e.g., the reviews in Refs. 3, 4). In molecular crystals with dipole-active excitonic transitions, which as a rule have higher values of oscillator strengths than those of semiconductors, the effect of exciton-photon mixing on the optical properties should be even more striking.

Among the molecular crystals, the anthracene crystal exhibits an anomalously large longitudinal-transverse splitting $\omega_{LT} \approx 400\ \text{cm}^{-1}$ and exciton effective mass $m_c^* \gtrsim 100\ m_e$ for the lower exciton band (by way of comparison, in crystals of CdS we have $\omega_{LT} = 15.4\ \text{cm}^{-1}$ for the A-excitons, while $m^* = 0.89\ m_e$, where m_e is the free electron mass[1]). This combination of parameters leads to a whole range of spectral and temporal peculiarities which affect the low-temperature luminescence[5–10] and kinetics of secondary emission under conditions of laser excitation.[11]

In this article we carry out a detailed study of the spectral content of secondary emission of anthracene crystals at low temperature under conditions of resonance excitation. We investigate the processes of propagation and scattering of polaritons which participate in the formation of the secondary emission spectrum. The numerical calculations we carried out are found to be in good quantitative agreement with our experimental results.

2. EXPERIMENTAL METHOD

The investigations were carried out on perfect single crystals of anthracene with extended [001] surfaces, grown by sublimation from zone-refined anthracene (~100 zones). The samples we used had thicknesses $d = 1.5$–40 μm. The low-temperature luminescence spectra of our crystals were identical to the ones presented in Ref. 12, and exhibited practically no bands corresponding to impurity emission. Simply supported samples were placed in an optical helium cryostat with a temperature regulator ($T = 1.5$–300 K).

As a source of excitation we used a pulsed tunable dye laser (VRO) with a tuning range $\omega_{ex} = 24\,000$–$26\,000\ \text{cm}^{-1}$ and an emission band with half width $\Delta\omega_{ex} = 1\ \text{cm}^{-1}$. Because it is easy to induce stimulated Raman scattering[13] in these crystals under resonance excitation conditions, the intensity of the laser pump was selected in such a way that the spontaneous-emission regime was ensured.

It should also be noted that there is a wide background of superradiance in the radiation from the tunable dye laser, especially in the short-wavelength region which is also the region of fundamental absorption of the anthracene crystal.

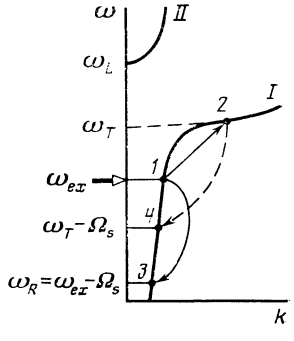

FIG. 1. Dispersion curve for polaritons; I—lower branch, II—upper branch. The following transitions are shown schematically: 1→2—anti-Stokes polariton scattering (occupied exciton band), 1→3—Stokes polariton RS, 2→4—exciton luminescence.

 0038-5646/88/122558-07$04.00

The presence of this superradiance can lead to a significant distortion in the spectral content of the emission under conditions of resonance excitation; therefore, we took special measures to ensure high monochromaticity of the tunable dye laser radiation. To accomplish this, we first directed the laser radiation at a dispersive element, which selected out an emission band; in this way, the superradiance background was eliminated.

The excitation light was directed along the normal to the surface of the crystal (along the $\mathbf{c}'$-axis) and was linearly polarized ($\mathbf{E}_{ex} \| \mathbf{b}$ – axis). The radiation spectrum was recorded using a DFS-24 spectrometer.

3. EXPERIMENTAL RESULTS

In Figs. 2a ($T = 1.9$ K) and 2b ($T = 5$ K) we show the emission spectrum of an anthracene crystal in the region of the optical transition involving the fully symmetric phonon with frequency 1403 cm^{-1} for various values of the frequency of the excitation light. It is easy to discern two groups of bands in the spectra. To the first group belong those bands whose spectral position (marked by the arrow in Figs. 2a, 2b) is independent of the frequency ω_{ex}; these bands correspond to well-known bands in the low-temperature exciton luminescence spectrum of perfect anthracene crystals.[5] The spectral position of the bands in the second group ω_R depends on the frequency ω_{ex} and is determined by the relation $\omega_R = \omega_{ex} - 1403$ cm^{-1}. Analogous results were also obtained for optical transitions involving high frequency phonons at 394, 1167, 1588 cm^{-1}, etc.

The general picture of the intensity variation of the bands in the first and second groups is shown in Fig. 3 for a crystal excited in the vicinity of the exciton resonance ω_T. The data in Figs. 2 and 3 show that only the exciton luminescence bands are observed in the emission spectra for values $\omega_{ex} \gtrsim \omega_T$.

A more complex structure is observed in the short-wavelength region of the emission spectrum (Fig. 4). Nevertheless, here too it is possible to identify two groups of bands—one group of bands corresponding to exciton luminescence (L) near the bottom of the exciton band ω_T, and another group (R) of bands whose spectral positions are determined by the relation $\omega_R^{(s)} = \omega_{ex} - \Omega_s$, where Ω_s is the

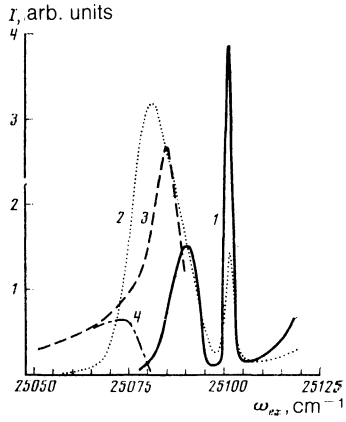

FIG. 3. Dependence of the intensity of the 23 692 cm^{-1} band in the exciton luminescence spectrum (traces 1 and 2) and the Stokes RS component due to the 1403 cm^{-1} phonon (traces 3 and 4) on the excitation light frequency ω_{ex} for two temperatures: 1, 3: $T = 1.9$ K, 2, 4: $T = 5$ K. The crystal thickness $d = 5$ μm.

frequency of the optical phonons at 49, 81, and 130 cm^{-1}. The index L' denotes bands corresponding to emission from an impurity center.[12]

Hence, the secondary emission spectra of anthracene crystals under conditions of resonance is a superposition of Raman light scattering (RS) spectra and exciton luminescence; the relative intensity of the spectrum depends significantly on the frequency ω_{ex} and the crystal temperature.

The influence of temperature on the intensity of the RS components (R) compared to the exciton component (L) of the emission spectra is visible in the data presented in Fig. 5, for two fixed values $\omega_T - \omega_{ex} = 60$ and 120 cm^{-1}. It is easy to see that as the temperature increases a sharp increase is observed in the intensity of the exciton luminescence, which is accompanied by a fall in the RS intensity. This behavior is also evident in the data in Figs. 2 and 3. As the frequency ω_{ex} decreases, the sharp increase in the exciton luminescence intensity is observed at higher temperatures. Figure 6 shows how the intensity $I_L^{(4)}$ of the luminescence band with fre-

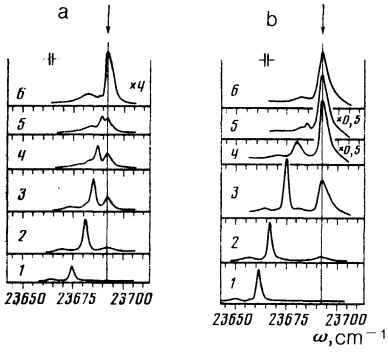

FIG. 2. Emission spectra of anthracene crystals in the frequency range $\omega \simeq \omega_T - 1403$ cm^{-1} for various values of $\omega_T - \omega_{ex}$: 1—20 cm^{-1}, 2—14 cm^{-1}, 3—9 cm^{-1}, 4—7.5 cm^{-1}, 5—6 cm^{-1}, 6— – 28 cm^{-1}, $T = 1.9$ K; (b) 1—33 cm^{-1}, 2—28 cm^{-1}, 3—20 cm^{-1}, 4—14 cm^{-1}, 5—9 cm^{-1}, 6— – 28 cm^{-1}, $T = 5$ K. The crystal thickness $d = 5$ μm. The arrow denotes the spectral position of the exciton luminescence band at 23 692 cm^{-1}.

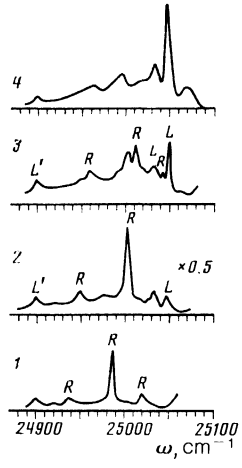

FIG. 4. Emission spectra of anthracene crystals near the bottom of the exciton band ω_T for various values of $\omega_T - \omega_{ex}$: 1—28 cm^{-1}, 2—14 cm^{-1}, 3—4 cm^{-1}, 4—excitation by the mercury line $\lambda = 365$ nm. The emission was recorded from the end of the crystal, $T = 1.9$ K, $d = 5$ μm.

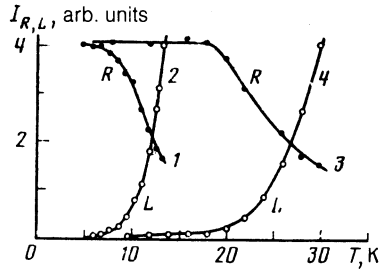

FIG. 5. Temperature dependence of the intensity of RS by the 1403 cm^{-1} phonon (R) and the luminescence (L) of the 23 692 cm^{-1} band for two values of $\omega_T - \omega_{ex}$: 1, 2—60 cm^{-1}, 3, 4—120 cm^{-1}.

quency $\omega_T - 1403$ cm^{-1} depends on the frequency ω_{ex} of the excitation light for the two temperatures $T = 1.9$ K and $T = 8$ K. Also noteworthy is the presence of structure (curve 2) in the region $\omega_{ex} = \omega_T - \Omega_1$; $\Omega_1 = 49$ cm^{-1} is the frequency of the lowest optical phonon. The value of $I_L^{(4)}$ approaches saturation as $\omega_{ex} \to \omega_T$; as we will show, this is because at certain values of ω_{ex} the light which excites the luminescence is absorbed in a layer smaller than the thickness of the crystal ($\varkappa d > 1$, where $\varkappa$ is the absorption coefficient).

The frequency dependence of the RS intensity for optical phonons $\Omega_s = 49$, 81, and 1403 cm^{-1} are shown in Fig. 7. As the frequency of the excitation light approaches resonance, i.e., $\omega_{ex} \to \omega_T$ ($\omega_T = 25\,096$ cm^{-1}) we first see a sharp growth in the intensity I_R which can approach two or more orders of magnitude as the value of ω_{ex} varies over a relatively narrow frequency interval $\omega_T - \omega_{ex} \lesssim 200$ cm^{-1}. The growth of the RS intensity is found to be sharper for the RS components with lower phonon frequencies Ω_s. In the immediate vicinity of resonance we observe a sharp intensity falloff for all RS components; in addition, bands corresponding to exciton luminescence appear in the emission spectrum. As the temperature is lowered, this falloff in intensity of the RS components and the concomitant appearance of exciton luminescence is observed for values of ω_{ex} further from resonance.

We now turn to an investigation of the processes which participate in the formation of the secondary emission spectrum.

4. RAMAN SCATTERING PROCESSES FOR POLARITONS BY OPTICAL AND ACOUSTIC PHONONS

At low temperature the magnitude of the longitudinal-transverse exciton splitting $\omega_{LT} \approx 400$ cm^{-1} for crystals of

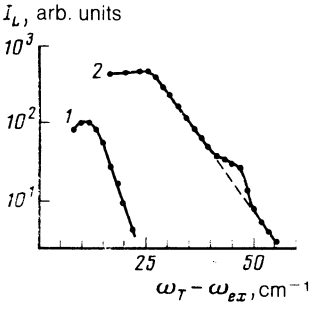

FIG. 6. Excitation spectrum of the 23 692 cm^{-1} luminescence band for various temperatures: 1—$T = 1.9$ K, 2—8 K; $d = 5$ μ.

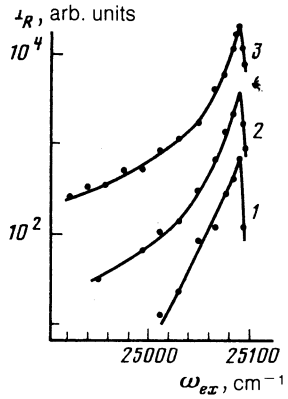

FIG. 7. Dependence of the intensity of the Stokes RS component from various optical vibrations Ω_s on the frequency of the excitation light: 1—49 cm^{-1}, 2—81 cm^{-1}, 3—1403 cm^{-1}; $T = 1.9$ K, $d = 5$ μm.

anthracene significantly exceeds the probability of decay of the exciton; for this reason, analysis of the secondary emission under conditions of resonant excitation is most conveniently carried out within the framework of the polariton representation.[14]

For later consideration, we introduce several equations which determine the various interaction processes between polaritons and phonons. It is well-known that the exciton component in the polariton excitation is determined by the strength function $S(\omega)$[15]:

$$S_\alpha(\omega) = \frac{\beta^2 \omega_\alpha(\mathbf{k})}{\omega(\mathbf{k})\left[(\omega_\alpha^2(\mathbf{k}) - \omega^2(\mathbf{k}))^2 + \beta^2\right]} \tag{2}$$

where

$$\beta^2 = \frac{\omega_p^2 F \omega_T^2}{\varepsilon_0} = 2\omega_{LT}\omega_T^3,$$

$\omega_\alpha(\mathbf{k})$, $\alpha = 1, 2$, are the upper and lower dispersive polariton branches, F is the oscillator strength of the transition, and ω_p is the plasma frequency. The frequency region where this component is close to unity is determined by the relation

$$\omega_T - \omega = \Delta\omega \lesssim (\omega_{LT}\omega_T)^{1/2} \tag{3}$$

for anthracene crystals this amounts to $\Delta\omega \approx 3000$ cm^{-1}.

It follows from the polariton model that the emission spectrum is produced by scattering processes between polaritons and phonons of various branches. The probability per unit time for scattering of a polariton of frequency ω by phonons from the s branch with emission $\gamma_s^{(+)}$ (Stokes scattering) or absorption $\gamma_s^{(-)}$ (Anti-Stokes scattering) of a phonon of frequency Ω_s is determined by the relation

$$\gamma_s^{(\pm)}(\omega) = \frac{2\pi}{\hbar}|F_s|^2 g(\omega \mp \Omega_s)\left(n_s + \frac{1}{2} \pm \frac{1}{2}\right), \tag{4}$$

where F_s is the matrix element for interaction of polaritons with phonons of the sth branch, n_s is the occupation number of phonons with frequency Ω_s, and $g(\omega \pm \Omega_s)$ is the spectral density of final states. The intensity of the Stokes component $I_R^{(s)}$ for scattering by a phonon Ω_s in a crystal of finite thickness d in the region of frequencies where the condition $kd \ll 1$ holds (k is the absorption coefficient determined by all the polariton scattering processes) is given by the relation

$$I_R^{(s)}=I_0 d/l_s, \tag{5}$$

where I_0 is the intensity of the exciton light, and l_s the mean free path of a polariton relative to Stokes RS by phonons Ω_s.

The magnitude of l_s is determined by the relation

$$l_s = V_g(\omega)/\gamma_s^{(+)}(\omega), \tag{6}$$

where $V_g(\omega)$ is the group velocity of the polaritons.

The optical phonons which participate in the polariton Stokes RS under discussion here have small values of quasimomentum $|\mathbf{q}_s| \ll \pi/a$ (a is the lattice constant); for these values of $\mathbf{q}_s$, the transitions in question are split, and the quantity $|F_s|^2$ is practically independent of $|\mathbf{q}|$. In addition, in the frequency region

$$\omega_T-\omega \lesssim 200\text{cm}^{-1} \ll (\omega_{LT}\omega_T)^{1/2}$$

the exciton component satisfies $S \approx 1$, and correspondingly the quantity

$$|F_s|^2 \propto S(\omega)S(\omega-\Omega_s)$$

also depends weakly on the frequency ω. Then for low temperatures ($n_s \ll 1$), the intensity of the polariton Stokes RS is given by

$$I_R^{(s)}(\omega) \propto g(\omega-\Omega_s)/V_g(\omega). \tag{7}$$

From this we see that the quantity $I_R^{(s)}$ is determined by the group velocity $V_g(\omega)$ and the density of final states $g(\omega-\Omega_s)$ in the resonance frequency region. We now pause to determine the frequency dependence of these parameters from the experimental data.

5. MEASUREMENT OF THE GROUP VELOCITY AND DETERMINATION OF THE DISPERSION CURVE PARAMETERS FOR THE LOWER POLARITON BRANCH

The dependence of the polariton group velocity on frequency for the lower polariton branch was measured by using the time-of-flight method.[16,17] In Fig. 8 we present the experimental results and numerical calculations of the group velocity $V_g(\omega) = \partial\omega/\partial k$ for several values of the effective mass m_c^*. In the course of these calculations we used the following relation for the dispersion of polaritons:

$$\frac{c^2k^2}{\omega^2} = \varepsilon_0 + \frac{\omega_p^2 F}{(\omega_T+\hbar k^2/2m_c^*-\omega)(\omega_T+\omega)}, \tag{8}$$

and the values $\varepsilon_0 = 2.7$, $\omega_p^2 = 2\cdot 10^8$ cm^2. The agreement between the calculated curves $V_g(\omega)$ and the experimental data allow us to find values for the parameters $\omega_T = 25\,096 \pm 0.5$ cm^{-1}, $F = 0.25 \pm 0.05$ and $m_c^* > 100\, m_e$.

Measurement of $V_g(\omega)$ also confirms assertions made earlier[7] concerning the fact that in the frequency range $\omega > \omega_T$ the minimum group velocity $V_g^{\min}(\omega)$ is found to be smaller then the velocity of sound, i.e., $V_g^{\min}(\omega) < u$; hence, in contrast to direct-gap semiconductor crystals, transitions from the region $\omega > \omega_T$ to the region $\omega < \omega_T$ with emission or absorption of one high-frequency acoustic phonon (transitions of the type 1↔2 in Fig. 1) are separated from their inverses.

6. NUMERICAL CALCULATIONS OF THE DENSITY OF POLARITON STATES

According to Ref. 7,

$$g(\omega) \propto \int d\varphi\, d\theta \sin\theta k^2(\omega,\varphi,\theta)\frac{\partial k(\omega,\varphi,\theta)}{\partial\omega}. \tag{9}$$

The functions $k^2(\omega, \phi, \theta)$ and $\partial k(\omega, \phi, \theta)/\partial\omega$ entering into (9) are determined by using the dispersion relation (1). The dependence of the exciton energy on wave vector k is applied in the form

$$\omega(\mathbf{k}) = \omega_T+\omega_{LT}\cos^2\theta + \frac{\hbar^2|\mathbf{k}|^2}{2}\left(\frac{\cos^2\varphi}{m_c^*}+\frac{\sin^2\varphi}{m_a^*}\right), \tag{10}$$

where θ is the angle between the vectors $\mathbf{k}$ and $\mathbf{b}$ and ϕ is the angle the vectors $\mathbf{k}$ and $\mathbf{c}'$; note that $\mathbf{b} \perp \mathbf{c}'$.

In Fig. 9 we present results of calculations for the various values of effective masses m_c^* and m_a^*. It is clear that in the immediate vicinity of resonance ($\omega_T - \omega \lesssim 10$ cm^{-1}) the jump in the density of polariton states can amount to several orders of magnitude, and that its value is determined

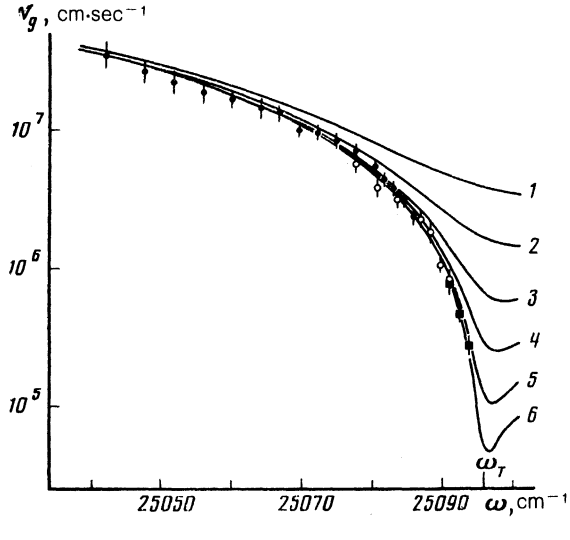

FIG. 8. Dependence of the group velocity $V_g(\omega)$ of polaritons on frequency, obtained for crystals of various thicknesses: ■—1.6 μm, ○—11.5 μm, ●—35 μm. The solid curves are calculated functions $V_g(\omega)$ for several values of effective mass m_c^*: 1—m_e, 2—3 m_e, 3—10 m_e, 4—30 m_e, 5—100 m_e, 6—300 m_e.

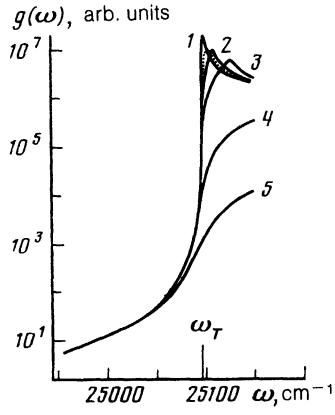

FIG. 9. Calculation of the polariton density of states $g(\omega)$ for various values of the exciton effective mass $m_a^* = m_c^*$: 1—1000 m_e, 2—300 m_e, 3—100 m_e, 4—10 m_e, 5—m_e. The dotted curve was obtained for $m_a^* = 300\, m_e$, $m_a^* = 1000\, m_e$, $F = 0.25$.

to a significant extent by the exciton effective mass. Decreasing the frequency leads to a decrease in the density of states; in the region of frequency $\omega_T - \omega > 50$ cm^{-1}, the value of the exciton effective mass has practically no effect on the character of the function $g(\omega)$ and the value of the group velocity $V_g(\omega)$.

7. COMPARISON OF THE EXPERIMENTAL RESULTS WITH NUMERICAL CALCULATIONS

It follows from our calculations that in the frequency region $\omega_R = \omega - 1403$ cm^{-1}, the change in the density of final states $g(\omega - \Omega_4)$ can be neglected as the frequency $\omega_T - \omega \lesssim 200$ cm^{-1} varies, and the frequency dependence of the intensity of the RS component takes the form

$$I_R \propto 1/V_g(\omega). \tag{11}$$

This relation describes the results of experiment to a high degree of accuracy up to frequencies $\omega_T - \omega \gtrsim 25$ cm^{-1} (Fig. 10). For the frequency range $\omega_T - \omega < 10$ cm^{-1}, at $T = 1.9$ K the condition of weak absorption $kd \ll 1$ is violated; because of this, it is necessary to use the exact relation in place of (11), taking into account the multiple transmission and reflection of polaritons excited in the plane-parallel crystal planes:

$$I_R^{(s)} = I_0 (kl_s)^{-1} (1-R) \frac{1-\exp(-kd)}{1-R\exp(-kd)}, \tag{12}$$

where R is the reflection coefficient. The quantity $(kl_s)^{-1}$ determines the fraction of polaritons undergoing Stokes RS by a phonon with frequency Ω_s, relative to the overall number of polaritons scattered in the crystal as a result of all processes of both Stokes and anti-Stokes scattering by optical and acoustic phonons.

Taking into account the variation in the magnitude of the absorption coefficient $\varkappa(\omega) < \varkappa(\omega)$ determines all the anti-Stokes polariton scattering processes) and reflection coefficient $R(\omega)$ with frequency, we can evaluate corrections to the intensity of the Stokes RS components in the frequency range $\omega > 25070$ cm^{-1} (the corresponding values $I_R^{(s)}$ are denoted by circles in Fig. 10). It is clear from Fig. 3 that a similar correction broadens the frequency range in which we observe agreement with the experimental functions $I_R(\omega)$ and $1/V_g(\omega)$ practically up to $\omega \approx \omega_T$.

It should be noted that if we no not include optical-exciton mixing, the dependence of the light intensity due to RS by phonons of the sth branch near resonance is primarily determined by a factor of the form[14]

$$I_R \propto [(\omega^2 - \omega_T^2)((\omega - \Omega_s)^2 - \omega_T^2)]^{-2}. \tag{13}$$

Curve 4 in Fig. 10 shows this function. It is clear that in this case there is a significant disagreement between the calculations and the experimental data.

Let us now investigate the processes of Stokes RS by phonons with $\Omega_s \ll \omega_{LT}$. In this case, calculations of $g(\omega)$ show that even in this frequency range it is not permissible to neglect the variation in the final state density. In Fig. 11, the solid trace is the frequency dependence of the intensity of the Stokes component for RS by $\Omega_1 = 49$ cm^{-1} phonons

$$I_{R\,\text{theor}}^{(1)} \propto g(\omega - \Omega_1)/V_g(\omega),$$

[$g(\omega - \Omega_1)$ is the calculated dependence of the final state density]; the points are from experiment. The circles, as in Fig. 10, denote corrected values of $I_R^{(1)}(\omega)$ near resonance, taking into account the coefficients $\varkappa(\omega)$ and $R(\omega)$. It is clear that agreement is good in this case.

Let us now investigate the anti-Stokes RS processes. At low temperatures ($T = 1.5$ to 10 K) these processes are determined by the probability of interaction with acoustic phonons Ω_s and (partially) with the low-frequency optical phonons $\Omega_1 = 49$ cm^{-1}. The interaction of polaritons with higher-frequency optical phonons does not give any contribution to the anti-Stokes RS processes, because their occupation number is negligibly small.

For anti-Stokes RS of polaritons we have

$$\gamma_s^{(-)} \propto g(\omega + \Omega_s)[\exp(\Omega_s/kT) - 1]^{-1}. \tag{14}$$

From this relation it follows that at fixed temperature there is a significant increase in probability for anti-Stokes RS in the immediate vicinity of resonance, which is essentially de-

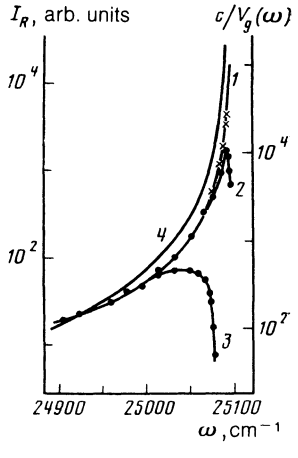

FIG. 10. Comparison of the experimental dependence of the intensity component of Stokes RS component by the phonon at 1403 cm^{-1} (2—$T = 1.9$ K and 3—$T = 10$ (K) with calculated values of $c/V_g(\omega)$ plotted as curve 1. The circles denote corrected values of $I_R^{(4)}$ taking into account the absorption and reflection coefficients. Curve 4 was calculated using Eq. (13).

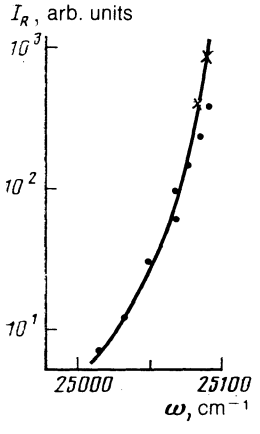

FIG. 11. Comparison of the experimental dependence of the intensity component of RS by the phonon at 49 cm^{-1} (black dots) with calculated values of $I_R^{(1)} \propto g(\omega - \Omega_1)/V_g(\omega)$ (solid curve).

termined by the sharp rise in the spectral density of final states in the region $\omega + \Omega \approx \omega_T$. Hence, as the polariton frequency increases, i.e., $\omega = \omega_{ex} \to \omega_T$, there results an occupation of the states near the bottom of the exciton band; in addition, bands of exciton luminescence appear in the emission spectrum along with the Stokes RS components. Up to this point, so long as the mean free path of the polaritons remains fairly large ($k^{-1}(\omega) \gg d$), the enhancement of the processes of anti-Stokes scattering by phonons leads only to a growth in intensity of the exciton luminescnce and leaves the character of the variation of the Stokes RS component intensity practically unchanged. Because the probability for anti-Stokes scattering $\gamma_s^{(-)}$ grows considerably more rapidly than the magnitude of the Stokes RS $\gamma_s^{(+)}$, as is apparent from the relation

$$\gamma_s^{(-)}/\gamma_s^{(+)} \propto g(\omega+\Omega_s)/g(\omega-\Omega_s), \tag{15}$$

the polariton mean free path begins to be essentially determined only by the anti-Stokes scattering processes as the frequency ω_{ex} increases, and eventually becomes comparable to or less than the thickness of the crystal ($k^{-1}(\omega) \approx \varkappa^{-1}(\omega) < d$). Since the opposite relation $l_s \gg d$ holds[10] for the mean free path of polaritons relative to Stokes scattering processes under our experimental conditions, enhancement of the anti-Stokes scattering leads to a falloff in the RS intensity I_R and eventual saturation of the exciton luminescence intensity. In this case it is easy to convince oneself with the help of (12) that for values $kd > 1$

$$I_R^{(s)} \approx I_0(1-R)/kl_s. \tag{16}$$

For frequencies $\omega_{ex} > \omega_T$, the quantity $k(\omega)$ attains a value for which $kl_s \gg 1$ ($\gamma_a^{(\pm)} \gg \gamma_s^{(+)}$), and the Stokes RS components practically disappear from the emission spectrum, so that the latter is entirely due to intrinsic exciton luminescence. In other words, with the enhancement of the anti-Stokes scattering processes there is a decrease in the effective region of the crystal ($k^{-1} > d$) in which Stokes RS can occur. The luminescence intensity in this case is determined only by the function $R(\omega)$:

$$I_L = I_0(1-R). \tag{17}$$

Our description of the transformation of the emission spectrum as $\omega \to \omega_T$ fully coincides with the experimental data in Figs. 3, 6, and 7.

Increasing the temperature leads to a growth in the phonon occupation numbers and an enhancement of the anti-Stokes RS, and correspondingly to a growth in the exciton luminescence intensity and a falloff in the Stokes RS component. The influence of temperature on the variation in spectral content of the emission is apparent in the results shown in Figs. 2, 3, and 5.

We also note that the observed structure (in the form of "steps") in the frequency dependence of the absorption coefficient for the region $\omega \approx \omega_T - \Omega_1$ (curve 2 in Fig. 6) points to the presence of a peak in the density of states near $\omega \approx \omega_T$, which agrees with the results of calculations of the density of states. Furthermore, the magnitude of the step (relative to the broken trace in Fig. 6) allows us to conclude that the processes of anti-Stokes scattering by acoustic phonons and by the optical phonon $\Omega_1 = 49\ \text{cm}^{-1}$ in the region $\omega_{ex} \approx \omega_T - \Omega_1$ are roughly equally probable, i.e., $\gamma_a^{(-)} \approx \gamma_1^{(-)}$. By making use of these facts, we can arrive at an estimate of the relative growth of the density of states $g(\omega)$ as the polariton frequency varies from $\omega \approx \omega_T - 2\Omega_1$ to $\omega \approx \omega_T$. Including the fact that the luminescent quantum efficiency for anthracene crystals is close to unity, the following relation can be shown to hold:

$$\frac{I_L(\omega-\Omega_1)}{I_R^{(1)}(\omega-\Omega_1)} \approx \frac{\gamma_a^{(-)}+\gamma_1^{(-)}}{\gamma_1^{(+)}} \approx \frac{2\gamma_1^{(-)}}{\gamma_1^{(+)}} \approx 2n(\Omega_1)\frac{g(\omega_T)}{g(\omega_T-2\Omega_1)}, \tag{18}$$

where $I_L(\omega - \Omega_1)$ is the luminescence intensity integrated over the spectrum when the frequency of the excitation light is $\omega_{ex} = \omega_T - \Omega_1$, and $n(\Omega_1)$ is the occupation number for optical phonons with $\Omega_1 = 49\ \text{cm}^{-1}$ at $T = 8$ K. Substituting into (18) the numerical values used in Figs. 2, 6, and 7, we obtain

$$g(\omega_T)/g(\omega_T-2\Omega_1) \approx (1.5 \pm 0.5) \cdot 10^6.$$

This value is found to be in good agreement with the calculated density of states (Fig. 9) when the exciton effective mass is chosen so that $m_c^* \gtrsim 300\ m_e$.

In conclusion, let us examine the character of the function $I_R(\omega)$ over a wide interval of frequency variation. In Fig. 12 we show the results of measuring $I_R^{(4)}$ in the frequency range $15800\ \text{cm}^{-1} < \omega_{ex} < 25\ 100\ \text{cm}^{-1}$, which were obtained using a tunable dye laser and discrete lines of HeCd, Ar^+ and HeNe lasers, along with the calculated values of $I_R^{(4)}$ taking into account the variation in $V_g(\omega)$, $S(\omega)S(\omega - \Omega_4)$, and $g(\omega - \Omega_4)$ in the entire frequency interval (curve 2 of Fig. 12).

Analysis of the experimental data and the calculation results shows that in the frequency range $\omega_T - \omega < 700\ \text{cm}^{-1}$ the change in $I_R^{(4)}$, which amounts to 4 orders of magnitude compared to its maximum value in the resonance region, is well described by invoking three simultaneous factors: the increase in group velocity $V_g(\omega)$, the decrease in the density of final states (which becomes significant for large values of the frequency ω), and also a roughly twofold falloff in the magnitude of $S(\omega)S(\omega - \Omega_4)$. However, over

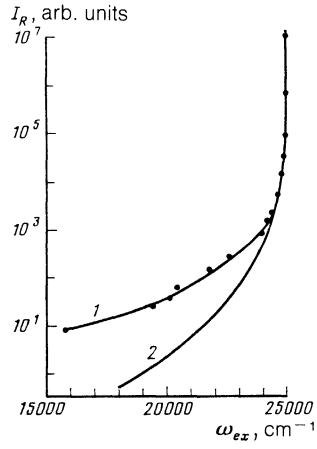

FIG. 12. Dependence of the intensity component $I_R(\omega)$ for Stokes RS by the phonon at 1403 cm^{-1} over a wide interval of measured ω_{ex}: 1—experimental data, 2—calculation.

the entire frequency interval ($\omega = 25\,100$ cm^{-1} to 16 000 cm^{-1}), in which the falloff of $I_R^{(4)}$ should amount to $\sim 5 \cdot 10^7$ according to calculations, the actual falloff of $I_R^{(4)}(\omega)$ turns out to be considerably less ($\sim 10^6$). This disagreement in the variation of the RS intensity $I_R^{(4)}(\omega)$ indicates that over a wide range of frequencies the application of Eq. (4) for an isolated resonance is not justified, and that for a quantitative comparison it is necessary to take into account contributions from higher energy electronic transitions, which, as is well known, possess quite large oscillator strengths.

8. CONCLUSIONS

To conclude, in this paper we have carried out a detailed investigation of the way the secondary emission spectrum of anthracene crystals changes as the optical excitation frequency varies within rather wild limits ($\omega_T - \omega_{ex} < 700$ cm^{-1}) near the lower exciton transition; in addition, we have delineated the effect of temperature on the spectral content of the radiation. All the results of our experiments can be consistently explained within the framework of the polariton representation. The numerical calculations we have carried out of the dependence of the intensity components of Raman scattering by various optical phonons ($\Omega_s \ll \omega_{LT}$ and $\Omega_s > \omega_{LT}$) are in good agreement with the experimental results.

[1]S. I. Pekar, *Kristallooptika i Dobavochnye Svetovye Volny* (*Crystal Optics and Additional Light Waves*, Benjamin, Reading, MA, 1983). Kiev: Nauk. Dumka, 1982.

[2]V. M. Agranovich and V. L. Ginzburg, *Kristallooptika c Uchetom Prostranstvennoi Dispersii i Teoriya Eksitonov* (*Spatial Dispersion in Crystal Optics, and the Theory of Excitons*, Wiley, New York, 1967). Moscow: Nauka, 1979.

[3]K. Weisbuch and R. Ulbrich, *Rasseyanie Sveta v Tverdykh Telakh* (*Light Scattering in Solids*), V. III. Moscow: Mir, 1985 (Berlin: Springer-Verlag), ch. VII.

[4]E. S. Koteles, *Eksitony* (Excitons, North-Holland, New York, 1982), Eds. E. I. Rashba and M. D. Sterdzha. Moscow: Nauka, 1985, ch. 3.

[5]M. S. Brodin, M. A. Dudinski, S. V. Marisova, and E. N. Myasnikov. Phys. Stat. Sol. (b) **74**, 453 (1976).

[6]J. Ferguson, Z. Phys.-Chem. **101**, 45 (1976).

[7]M. D. Galanin, Sh. D. Khan-Magometova, and E. N. Myasnikov, Mol. Cryst. Liq. Cryst. **57**, 119 (1980).

[8]N. A. Vidmont, A. A. Maksimov, and I. I. Tartakovskii, Fiz. Tverd. Tela (Leningrad) **24**, 1384 (1982) [Sov. Phys. Solid State **24**, 784 (1982)].

[9]A. Aaviksoo, G. Liidja, and P. Saari, Phys. Stat. Sol. (b) **110**, 69 (1982).

[10]N. A. Vidmont, A. A. Maksimov, and I. I. Tartakovskii, Izv. Akad. Nauk SSSR, Ser. Fiz. **47**, 1296 (1983) [Bull. Acad. Sci. USSR, Phys. Ser. (unavailable)].

[11]J. Aaviksoo, A. Frieberg, T. Reinot, and S. Savikhin, J. Lumin. **35**, 267 (1986).

[12]E. Glokner and H. C. Wolf, Z. Naturforsch. A **24**, 943 (1969).

[13]A. A. Maksimov, and I. I. Tartakovskii, Phys. Stat. Sol. (b) **107**, 55 (1981).

[14]B. Bendow, *Springer Tracts in Modern Physics* **82** (Berlin: Springer-Verlag, 1978), p. 69.

[15]V. M. Agranovich and M. D. Galanin, *Perenos Energii Elektronnogo Vozbuzhdeniya v Kondendirovannykh Sredakh Electronic Excitation Energy Transfer in Condensed Media*, North-Holland, Amsterdam (1982). Moscow: Nauka, 1978.

[16]N. A. Vidmont, A. A. Maksimov, and I. I. Tartakovskii, Pis'ma Zh. Eksp. Teor. Fiz. **37**, 578 (1983) [JETP Lett. **37**, 689 (1983)].

[17]J. Aaviksoo, J. Lippmaa, A. Freidberg, and A. Anifalg, Solid State Commun. **49**, 115 (1984).

Translated by Frank J. Crowne